PHYSICAL REVIEW B VOLUME 7, NUMBER 10 15 MAY 1973

Properties of 1.0-MeV-Electron-Irradiated Defect Centers in Silicon[*]

J. W. Walker[†] and C. T. Sah

Departments of Electrical Engineering and of Physics, and Materials Research Laboratory,
University of Illinois, Urbana, Illinois 61801

(Received 5 September 1972)

The presence of electrically active defects in 1.0-MeV-electron-irradiated silicon was observed using thermally stimulated capacitance measurements. Thermal-emission rates and activation energies of trapped majority carriers, impurity dependences, and annealing behavior of these defects were determined. The introduction of defects by annealing was observed. A total of 14 thermal-activation energies were measured. The oxygen-vacancy pair and the phosphorous-vacancy pair were correlated with thermal-activation energies of 174 and 471 meV through impurity dependences and annealing behavior. Comparison with other published data was made. The charge states were measured and it was found that the defects above midgap are acceptors; those below midgap are donors.

I. INTRODUCTION

Bombardment of silicon with electrons of energy 1 MeV introduces a variety of defects into the lattice. There have been many studies to determine the properties of these defects. Hall-effect measurements,[1–10] minority-carrier-lifetime studies,[11–18] and infrared photoconductivity and adsorption measurements[19–23] have been made to determine the spectrum of energy levels introduced in the forbidden energy gap. Electron-spin resonance has been used very successfully to determine the microscopic configuration of several defects.[24–28] The results of these studies are summarized in Table I. Generally, not all of the levels were observed in each of these studies. It is known that, in some cases, more than one defect is responsible for an observed energy level.

It is the purpose of this paper to report the defect inventory observed in 1-MeV-electron-irradiated silicon using the methods of thermally stimulated capacitance[29,30] and isothermal junction current and capacitance transients.[31] These methods allow the detection of all electrically active defects with energy levels within the forbidden gap, with a detection sensitivity of better than 0.1% of the total defect concentration. The impurity dependence, charge state, and annealing behavior of each defect are determined. No defects with multiple charge states were observed, since there were no correlations between the introduction and annealing rates. These results are compared with those of other investigators.

The results on p-type silicon have been previously reported.[32] They are included here for comparison with the n-type results.

II. MEASUREMENT METHODS

A. Theory

The presence of deep-level[33] defects in a semiconductor can be detected by observing the capture and emission of charge carriers at the defect site. This can be done by monitoring the reverse-bias capacitance of a p-n junction after disturbing the steady-state charge condition. The following description is divided into three parts: (i) capture and emission of charge carriers at defect sites in a depletion region; (ii) observing emission of charge carriers by monitoring reverse-bias capacitance; and (iii) disturbing the steady-state charge concentration.

(i) The four processes by which the charge state of a deep-level defect is changed, according to the Shockley–Read–Hall[34] model, are illustrated in Fig. 1. Process (a) represents electron capture and is characterized by the electron-capture rate c_n^t. Process (b) represents electron emission and is characterized by an electron thermal-emission rate e_n^t. Process (c) and (d) represent hole capture and hole emission similarly. (It will be assumed throughout the paper that these processes are thermally activated. This is true since the sample was shielded from any optical excitation by the cold walls of the sample holder.)

The net rate of change of the concentration of trapped electrons, n_T, or holes, p_T, is obtained by summing the contribution from each of the four processes as follows: (a) electron-capture rate, represented by $c_n^t n p_T$; (b) electron-emission rate, represented by $e_n^t n_T$; (c) hole-capture rate, represented by $c_n^t p n_T$; and (d) hole-emission rate, represented by $e_n^t p_T$;

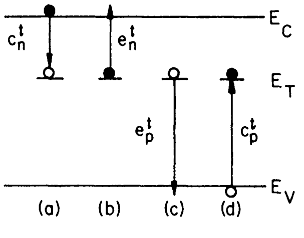

FIG. 1. Charge-state changes at deep-level defects.

TABLE I. Summary of studies of radiation-damaged silicon.

ΔE (eV)	Reference (No.)	Comments
$E_C - 0.12 \pm 0.02$	3, 10, 12, 51	appears in low-oxygen material
$E_C - 0.17 \pm 0.02$	1, 2, 5, 8, 10–16, 19, 23, 25	correlated with oxygen-vacancy pair
$E_C - 0.22 \pm 0.01$	19, 14, 5, 21	introduction by annealing observed (Ref. 5)
$E_C - 0.42 \pm 0.06$	2, 3, 5, 8, 16, 21, 23, 25, 26	correlated with phosphorus-vacancy pair (5, 25, 26) and with divacancy (21)
$E_C - 0.52 \pm 0.02$	15, 21, 23	may be related to divacancy (21, 23)
$E_V + 0.40 \pm 0.05$	14, 11, 21–23, 28, 7	correlated with acceptor-defect complexes (22), oxygen dependence observed (7)
$E_V + 0.28 \pm 0.02$	1, 2, 4, 6–8, 14, 15, 17, 20, 21, 25, 28	correlated with divacancy (21, 25) and with *K* center (25); oxygen dependence observed (4, 8); acceptor dependence observed (6); oxygen independence (6, 7, 17); acceptor independence observed (8, 9)
$E_V + 0.20 \pm 0.02$	4, 7, 9, 15, 17, 20, 28	correlated with divacancy (28), room-temperature annealing observed (23)

$$\frac{dn_T}{dt} = -e_n^t n_T + c_n^t n p_T + e_p^t p_T - c_p^t p n_T = -\frac{dp_T}{dt} , \quad (1)$$

where $n(p)$ is the free-electron (-hole) concentration, $n_T(p_T)$ is the trapped-electron (-hole) concentration, $e_{n(p)}^t$ is the electron (hole) thermal-emission coefficient, and $c_{n(p)}^t$ is the electron- (hole-) capture coefficient. This equation is simplified in the depletion region of a *p*-*n* junction, where the carrier concentrations are negligible, $n \simeq p \simeq 0$. With this approximation, Eq. (1) becomes

$$\frac{dn_T}{dt} = -e_n^t n_T + e_p^t p_T = -\frac{dp_T}{dt} . \quad (2)$$

Using $n_T + p_T = N_{TT}$, which is the total concentration of a deep-level defect, the solution of (2) is

$$\Delta n_T(t) = \Delta n_T(0)\, e^{-(e_n^t + e_p^t)t}, \quad (3)$$

where Δn_T is the disturbance of the trapped-electron concentration from its steady-state value. This disturbance is seen to decay exponentially with a time constant given by the reciprocal of the sum of the thermal-emission rates, $e_n^t + e_p^t$. It has been shown in other measurements[35–38] that these emission rates vary exponentially with temperature, $e^t \sim e^{-\Delta E/kT}$, where ΔE is the thermal-activation energy and approximately the energy level from a band edge.[39]

The measurements to be described here follow from Eq. (3) together with the exponential temperature dependence of the emission rates. The presence of deep-level defects is determined by observing the presence of the decay implied by Eq. (3). Measurements of this decay versus temperature yield values for the activation energy of thermal emission of trapped carriers.

(ii) The emission of charge carriers from defect sites in a depletion region is observed by monitoring the capacitance of the depletion region. The capacitance of a reverse-biased *p*-*n* junction in the depletion approximation is given[40] by

$$C^2 = \epsilon\rho/2(V_R + V_B), \quad (4)$$

where ϵ is the semiconductor dielectric constant, V_B is the magnitude of the built-in voltage, V_R is the magnitude of the reverse-bias voltage, and ρ is the magnitude of the fixed charge density in the depletion region. For the *n*-type side of a p^+n diode with a deep-level acceptor,

$$\rho = q\,[N_D - n_T(t)] . \quad (5)$$

This illustrates that ρ is time and temperature dependent due to the emission of trapped charges at the deep-level defects. The capacitance of a reverse-biased diode will show a similar dependence since it is proportional to $\rho^{1/2}$.

(iii) There are many ways to disturb the steady-state charge concentration in a depletion region.[31] The method employed here will be discussed with the aid of Fig. 2. In the quasineutral and nearly-

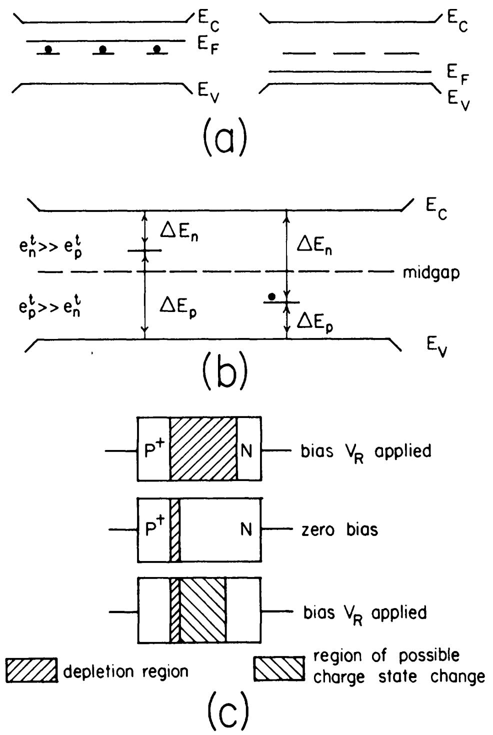

FIG. 2. Method of disturbing steady-state charge in the depletion region.

thermal-equilibrium region of a diode, the charge state of the trap is determined by the detailed balance of the electron-capture and emission processes [see Fig. 2(a)]. At the low temperatures of measurement, the Fermi level is near one of the band edges. Therefore, electrons are trapped at defects in n-type silicon and holes are trapped at defects in p-type silicon. In the highly nonequilibrium depletion region of the junction, the capture rates are zero, and the charge state of the defects are determined by the relative emission rates of electrons and holes. Due to the exponential dependence of the emission rates on the activation energy, $e_{n(p)} \sim e^{-\Delta E_{n(p)}/kT}$, the steady-state charge concentration of a defect corresponds to holes trapped at levels below midgap and electrons trapped at levels above midgap [see Fig. 2(b)]. Defects may be switched from a depletion region to a quasineutral region and switched back by momentarily zero biasing a reverse-biased diode as illustrated in Fig. 2(c). This process disturbs the steady-state charge concentration in the depletion region when the charge state of a defect in the neutral region differs from the steady-state charge in the depletion region. Table II shows the combinations of defect levels and type of diode which allow charge-state change by momentary zero bias. From this table, it is seen that defects with energy levels above midgap may be observed in diodes with n-type substrates and those with levels below midgap may be observed with p-type substrates. By studying both diode types, the entire band gap can be scanned for defect energy levels.

TABLE II. Charge-state change by momentary zero bias.

Defect levels	p^+n	n^+p
$E_T >$ midgap	yes	no
$E_T <$ midgap	no	yes

Two types of experiments using these effects have been performed on 1-MeV-electron-irradiated silicon. Figure 3 illustrates these experiments for the case of a p^+n diode with deep-level acceptors. The first of these experiments, thermally stimulated capacitance (TSCAP), allows a rapid scan of all the deep-level defects which are majority-carrier (electrons in p^+n diodes) traps on the lowly doped side. The diode is cooled to a temperature such that the emission rates are negligible. The diode is zero-biased momentarily and then heated at a constant rate. In a characteristic temperature range related to the emission activation energy, the emission rate becomes large enough for all the trapped electrons to be thermally emitted to the conduction band and swept out of the depletion region. This results in an increase in the charge concentration in the depletion region and a corresponding capacitance increase. There will be one of these capacitance steps for each activation energy in the upper half of the band gap.

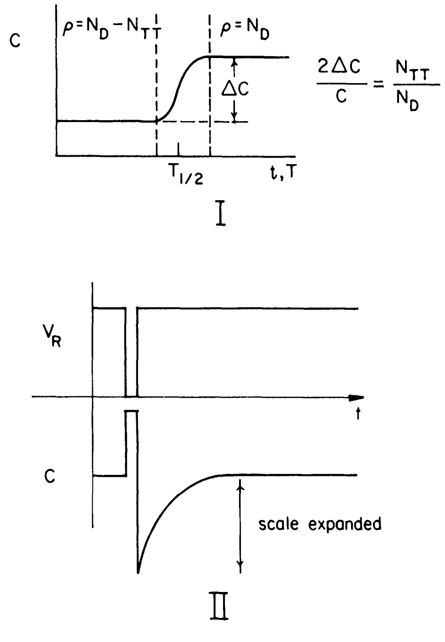

FIG. 3. Experiments.

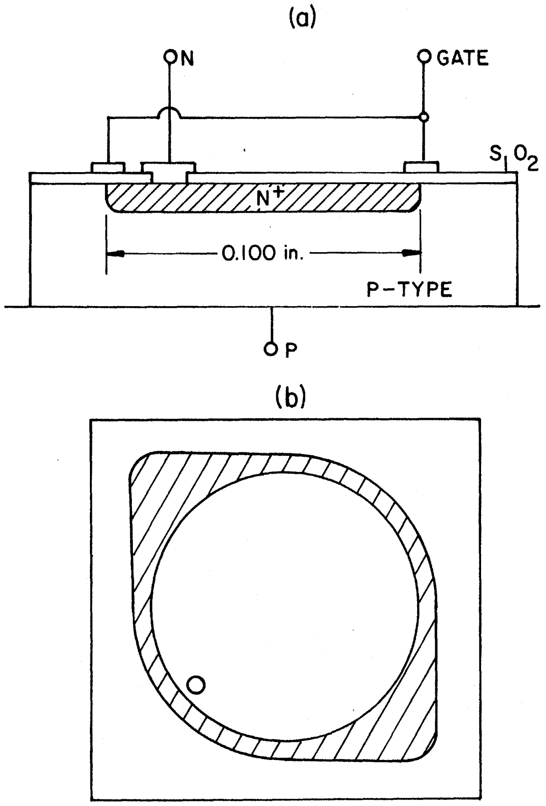

FIG. 4. Diode geometry.

The magnitude of each step can be shown[29] to be related to the concentration of defects producing the step

$$2\Delta C/C = N_{TT}/N_D, \quad (6)$$

where ΔC is the magnitude of capacitance step, C is the capacitance after electron emission, N_{TT} is the concentration of defects, and N_D is the concentration of shallow-level doping impurities obtained from C^{-2} versus V_R.[40] This equation is valid for $N_{TT} \leqq 0.1 N_D$. TSCAP measurements made on both types of diodes allow a rapid inventory of the electrically active defects.

The second experiment, emission-rate measurements versus temperature, allows the determination of the activation energy of each defect. It can be shown,[31] using Eqs. (3)–(5), that after a momentary zero bias, the capacitance exhibits an exponential transient having a time constant given by the reciprocal emission rate of the trapped majority carriers (electrons),

$$\Delta C \sim e^{(-e_n^t t)}, \quad (7)$$

where it is assumed that $e_n^t \gg e_p^t$. Measurements of this transient at various temperatures show an exponential temperature dependence,

$$e_n^t = A_n(\tfrac{1}{300}T)^m e^{-\Delta E/kT}, \quad (8)$$

where m cannot be determined from the experiment. The data are least-squares fitted to Eq. (8) to give the thermal-activation energy for $m = -1$, 0, 1, and 2. Results for $m = 2$ will be quoted in the text for reasons to be discussed.

B. Experimental Details

Figure 4 shows the diode geometry used in these measurements. They were fabricated using standard diffusion techniques. n^+p diodes were fabricated by the diffusion of phosphorus into boron-doped Czochralski-grown silicon. p^+n diodes were fabricated by diffusing boron into phosphorus-doped Czochralski-grown silicon. The gate electrode was used to monitor and control surface channels. The diodes were bonded on TO-5 headers at 400 °C for 30 sec before irradiation in order to avoid annealing effects if post irradiation bonding is employed. The residual deep-level-defect concentration before irradiation was measured by the low-temperature high-frequency capacitance method[41] and found to be of the order of 2×10^{11} cm^{-3} or less.

For the study of oxygen effects on defect formation, float-zone silicon was used with an oxygen concentration about 100 times less than in Czochralski-grown silicon. To avoid oxygen doping during the high-temperature junction-diffusion process, Schottky-barrier diodes were fabricated on the float-zone material by evaporating 0.030-in.-diam aluminum dots on chemically polished slices. The junction is then sintered at a temperature of 550 °C for 15 min in a dry-argon atmosphere. The properties of the diodes used in this paper are given in Table III.

The diodes were irradiated in vacuum at room temperature with 1-MeV electrons at a current of 2.0 μA/cm^2 using the Van de Graaff accelerator located at the Materials Research Laboratory of the University of Illinois. The irradiation sample holder is shown in Fig. 5. The electron beam was collimated by a series of apertures and struck the diode mounted in a Faraday cup. The total dose was determined by integrating the current from the Faraday cup using an Elcor Model No. 309B current indicator and integrator. The dose was adjusted so

TABLE III. Diode types used in this study.

Diodes	Type	Substrate, (111) oriented
72871*A*	n^+p	1.0×10^{14} boron/cm^3, Czochralski
72871*B*	n^+p	4.0×10^{14} boron/cm^3, Czochralski
72871*C*	n^+p	4.0×10^{14} boron/cm^3, Czochralski
72871*D*	n^+p	9.0×10^{14} boron/cm^3, Czochralski
61071*B*	p^+n	5.0×10^{14} phosphorus/cm^3, Czochralski
61071*C*	p^+n	5.0×10^{15} phosphorus/cm^3, Czochralski
61071*D*	p^+n	5.0×10^{14} phosphorus/cm^3, Czochralski
22272*A*	p^+n	5.0×10^{13} phosphorus/cm^3, Czochralski
22272*B*	p^+n	5.0×10^{13} phosphorus/cm^3, Czochralski
42772*A*	Schottky	7.0×10^{13} phosphorus/cm^3, float zone

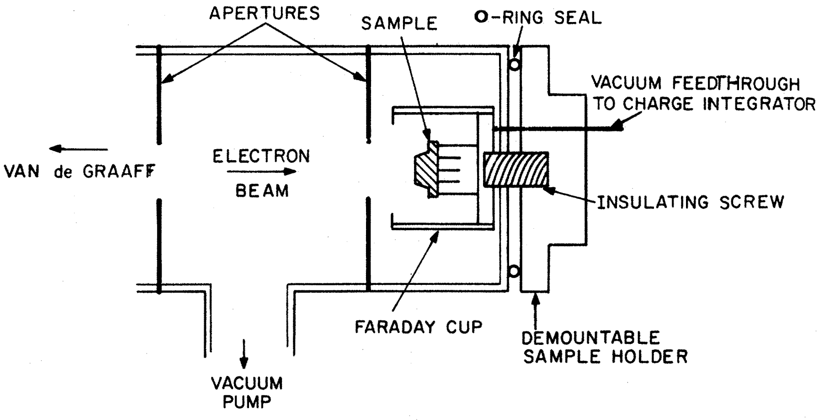

FIG. 5. Irradiation sample holder.

that the total defect concentration introduced was about 0.2 times the doping impurity concentration. It is estimated that the temperature rise of the diode during irradiation was less than 10 °C. For some irradiations carried out at 20 $\mu A/cm^2$, the temperature rise exceeded 25 °C. The diodes were stored in liquid nitrogen immediately after irradiation.

The capacitance measurements were made using a Boonton Model No. 71A direct-reading capacitance meter with a 1.0-MHz 15-mV measuring signal. The analog output of the Boonton meter was recorded on a Hewlett Packard Model No. 7100B strip-chart recorder. The temperature was measured to ± 0.2 °K.

III. EXPERIMENTAL RESULTS

After room-temperature irradiation of n^+p and p^+n diodes, the following measurements were made: (i) TSCAP measurements to determine the number of activation energies in the appropriate half of the band gap (see Table II); (ii) emission rate versus temperature to accurately determine the activation energies; (iii) introduction rates versus impurity concentrations to determine impurity dependences of the defects.

A. Room-Temperature Irradiation: *p*-type (Ref. 32)

(i) A TSCAP measurement made on an irradiated n^+p diode shortly after irradiation is illustrated in Fig. 6 (no steps were observed for $T < 77$ °K). The capacitance-meter output was recorded versus time or thermocouple emf. Curve *b* reveals the presence of three activation energies in the lower band gap. Curve *a* was taken without zero biasing, so that no holes are trapped. The temperature dependence of curve *a* is due to bulk Fermi level crossing the trap level in the edge region.[49] Curves *a* and *b* were subtracted to yield the capacitance changes from hole emission in the depletion region. Individual defect concentrations were obtained by using the measured capacitance changes as described by Eq. (6).

In the text following, a capacitance step will be identified by the temperature $T_{1/2}$, at which the capacitance change reaches one-half of its maximum. $T_{1/2}$ corresponds roughly to the temperature at which the peak occurs in thermally stimulated current[29] or dC/dt measurements.[32]

(ii) The activation energies of the defects observed in this TSCAP measurement were determined by measuring the emission rates as a function of temperature. The results of these measurements are given in Fig. 7. (The emission rates greater than 1.0 sec^{-1} were determined from

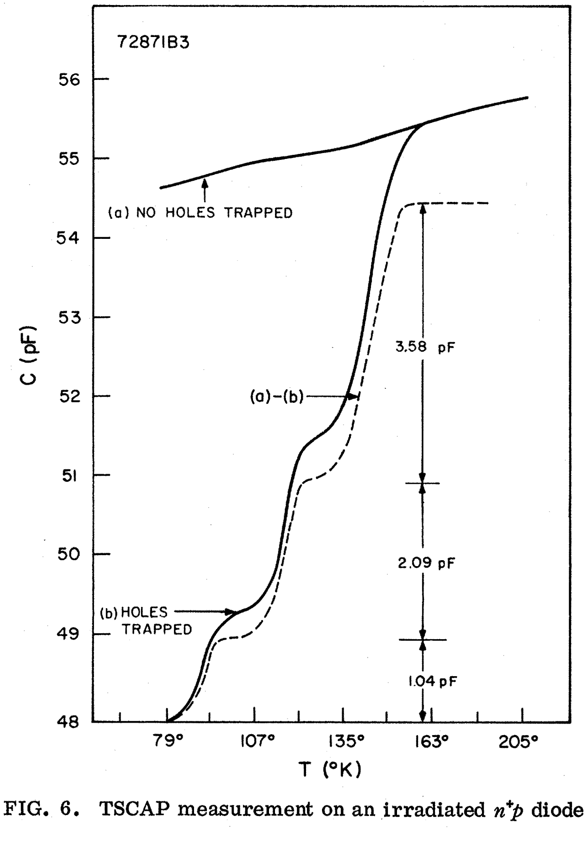

FIG. 6. TSCAP measurement on an irradiated n^+p diode.

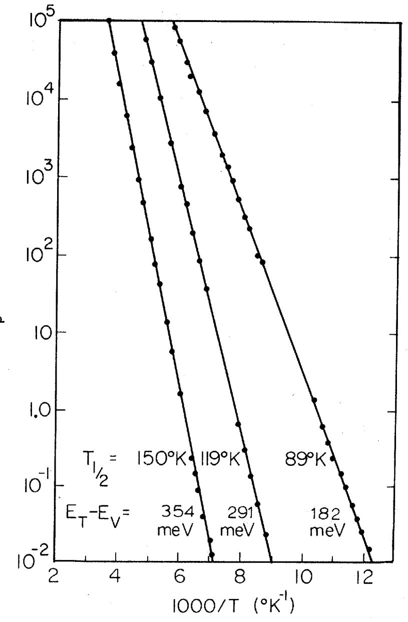

FIG. 7. Hole-emission rates from defects present after room-temperature irradiation.

transients in the reverse current.[31]) The curves are labeled with the activation energy obtained from a least-squares fit of the data to Eq. (8) with $m = 2$. The results for other values of m are tabulated in Table IV. The tolerances listed are indicative of how well the given curve fits the experimental data. It can be seen from Table IV that each value of m fits the data about equally well and that the thermal-activation energy varies considerably from one value of m to another. The $m = 2$ values are quoted in the text for reasons to be discussed.

TABLE IV. Least-squares-fit parameters for different powers of T in the preexponential factor for hole traps present after room-temperature irradiation (tolerances indicated are 70% fiducial limits): $e_p^t = A_p^t(\frac{1}{300}T)^m e^{-\Delta E/kT}$.

m	ΔE(meV)	A_p^t
$E_T - E_V = 354$ meV, A_p^t units $= 10^{11}$ sec^{-1}, $T_{1/2} = 150$ °K		
2	354.1 ± 0.7	2.37 ± 0.12
1	369.7 ± 0.9	3.89 ± 0.24
0	385.6 ± 1.2	6.62 ± 0.53
−1	401.3 ± 1.4	11.12 ± 1.08
$E_T - E_V = 291$ meV, A_p^t units $= 10^{12}$ sec^{-1}, $T_{1/2} = 119$ °K		
2	290.7 ± 0.8	1.30 ± 0.09
1	304.0 ± 0.9	1.81 ± 0.14
0	316.6 ± 1.1	2.54 ± 0.23
−1	329.5 ± 1.3	3.55 ± 0.39
$E_T - E_V = 182$ meV, A_p^t units $= 10^{10}$ sec^{-1}, $T_{1/2} = 89$ °K		
2	181.6 ± 0.5	5.99 ± 0.27
1	197.5 ± 0.5	6.49 ± 0.33
0	207.4 ± 0.6	7.04 ± 0.41
−1	217.4 ± 0.8	7.64 ± 0.53

TABLE V. Introduction rates of defects with energy levels below midgap measured in n^+p diodes with different substrate boron concentrations.

N_{boron} (cm^{-3})	Diode	$(N_{354} + N_{291})/\Phi$ (cm^{-1})	N_{182}/Φ (cm^{-1})
1.1×10^{14}	72871*A*7	0.0289	0.0030
	72871*A*8	0.0280	0.0042
	12771*B*11	0.0214	0.0032
	12771*B*7	0.0222	0.0028
4.2×10^{14}	72871*B*3	0.0212	0.0035
	72871*C*12	0.0244	0.0051
	72871*B*5	0.0281	0.0020
	72871*B*10	0.0214	0.0033
8.8×10^{14}	72871*D*4	0.0268	0.0042
	72871*D*7	0.0250	0.0040
	72871*D*10	0.0260	0.0043

(iii) The boron dependence of these defects was investigated by measuring their introduction rates in diodes with various boron concentrations. The results are shown in Table V. The introduction rates were determined by dividing the concentrations obtained from TSCAP measurements by the integrated electron flux Φ. The 354- and 291-meV defects were added because of their room-temperature annealing behavior to be discussed. The table shows that the introduction rates are not related to the boron concentration, implying that these defects are not boron-defect complexes.

B. Room-Temperature Irradiation: *n*-type

(i) TSCAP measurements on p^+n diodes fabricated on Czochralski-grown substrates are illustrated in Figs. 8 and 9. Figure 8 was obtained with the diode in a liquid-helium Dewar; Fig. 9 in a liquid-nitrogen Dewar. One activation energy is observed in Fig. 8; three in Fig. 9. The decrease in the capacitance below 40 °K in Fig. 8 is due to the freeze-out of electrons on the shallow-level phosphorus atoms. The capacitance decrease in curve *a* in Fig. 9 below 170 °K is related to the presence of the level indicated in Fig. 8. As the temperature is lowered, the Fermi level rises in the gap, eventually crossing the energy level of the 70 °K defect shown in Fig. 8. Electrons are frozen onto this defect, reducing the free-electron concentration near the edge of the depletion region causing a decrease in the capacitance.[49]

By comparing the size of the steps in Figs. 8

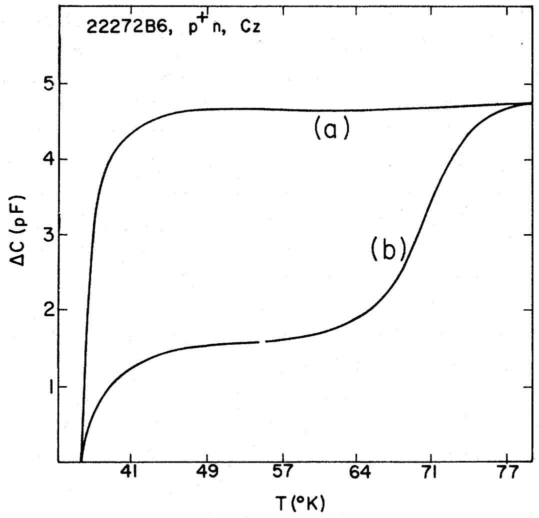

FIG. 8. TSCAP measurement on an irradiated p^+n Czochralski diode, $T < 77$ °K.

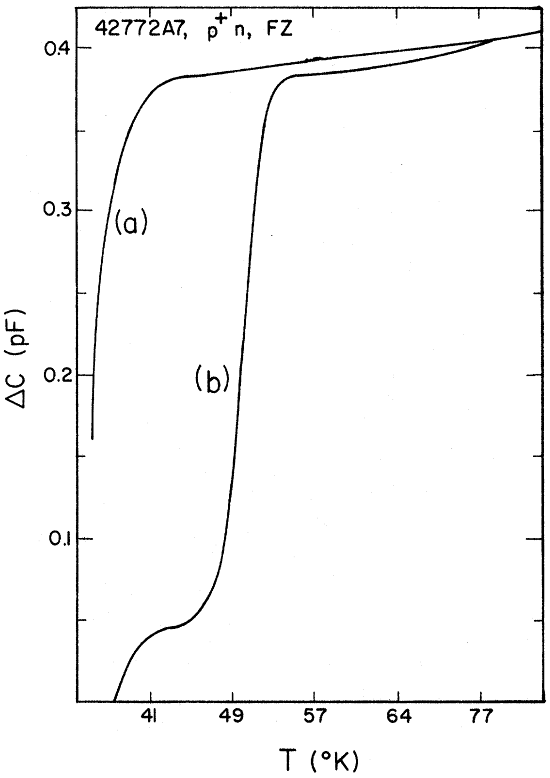

FIG. 10. TSCAP measurement on an irradiated p^+n float-zone diode, $T < 77$ °K.

and 9, it can be seen that the damage in these diodes is dominated by the step occurring at 70 °K. Preliminary determinations[29] of the activation energy yielded a value near that associated with the oxygen-vacancy pair. The defects in Fig. 9 could be more easily studied if their concentrations are higher and comparable to the 70 °K level in Fig. 8. This could be accomplished by reducing the oxygen-vacancy introduction rate by using float-zone-refined silicon. The Schottky-barrier diodes were fabricated on float-zone material for this purpose. (An attempt was made to diffuse a junction in float-zone material. Measurements of oxygen-vacancy concentration after irradiation indicated that oxygen had diffused over 30 μ into the sample.)

Thermally-stimulated capacitance curves obtained after the irradiation of these float-zone diodes are shown in Figs. 10 and 11. Several differences between float-zone and Czochralski material are readily evident. A new defect is observed in Fig. 10 at $T = 50$ °K, while the defect at 203 °K observed in the Czochralski crystal in Fig. 9 is missing. The concentration of the defect at 70 °K is reduced in the float-zone diodes, confirming that it is oxygen related. (The area of the float-zone diodes is one-tenth the area of the Czochralski diodes.) The steps in Fig. 11 have

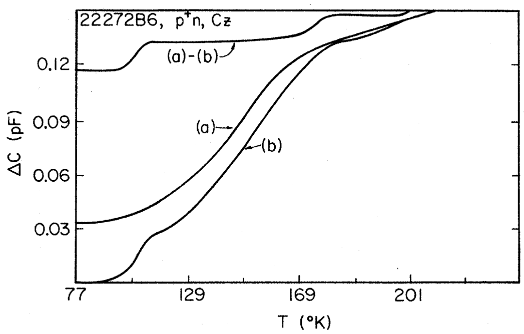

FIG. 9. TSCAP measurement on an irradiation p^+n Czochralski diode, $T > 77$ °K.

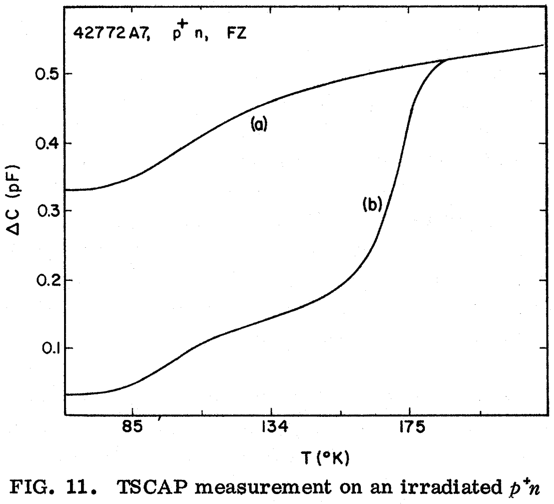

FIG. 11. TSCAP measurement on an irradiated p^+n float-zone diode, $T > 77$ °K.

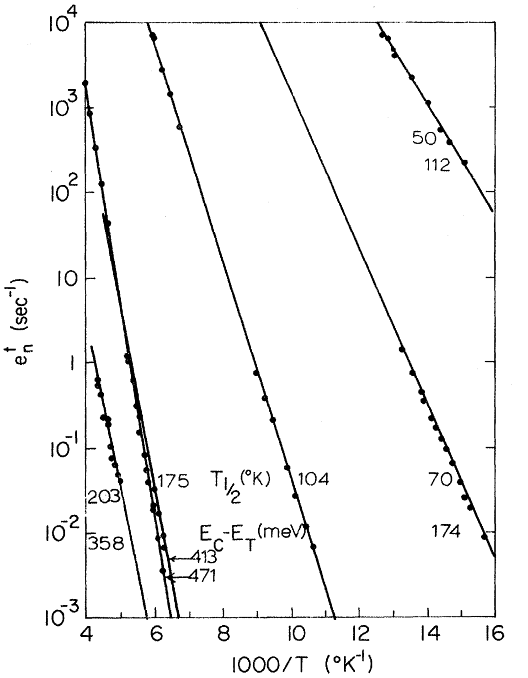

FIG. 12. Electron emission rates from defects present after room-temperature irradiation, $T > 63$ °K.

the same relative magnitude as the steps in Fig. 10, achieving nearly equal concentration for all the defects introduced.

(ii) The thermal-emission rates of electrons at the defect centers corresponding to the capacitance steps in Figs. 8–11 were measured versus temperature. The results appear in Figs. 12 and 13. The curves are labeled with the temperature at which the steps occur and with the activation energy obtained from Eq. (8) with $m = 2$. (The capacitance transient related to the 70 °K step was nonexponential. The data presented here were obtained by taking the reciprocal of the time required for the capacitance change to decay by a factor of $1/e$.)

The contents of Figs. 12 and 13 require some explanation. Two slopes are observed related to the step at 175 °K. The slope of 413 meV was observed in Czochralski diodes having a low phosphorus concentration. The slope of 471 meV was observed in float-zone diodes and in Czochralski diodes with high phosphorus concentration. This implies that there are probably two different defects contributing to this capacitance step, one phosphorus related and one independent of phosphorus.

The slopes of the data related to the 104 and 70 °K steps appear to be independent of the diode type. The 203 °K center is observed only in Czochralski diodes and the 50 °K center is observed only in the float-zone diodes.

These data were least-squares fitted to Eq. (8) with the results as indicated in Table VI. The large error limits on some of the data are the result of small defect concentrations.

(iii) The oxygen and phosphorus dependence of these defects may be determined by measuring the introduction rates in float-zone silicon and in Czochralski silicon with various phosphorus concentrations. The results of the introduction-rate measurements are given in Table VII.

Looking first at the results of measurements on Czochralski diodes, it is seen that the 70 (174 meV) and 104 °K (236 meV) centers are independent of the phosphorus concentration. The data on the 203 °K (358 meV) center are not sufficiently accurate to be interpreted. The 175 °K capacitance step again shows evidence of the effects of two types of defects; it is independent of phosphorus at small concentrations, but its introduction rate increases at high phosphorus concentrations. This is further evidence of the contributions to this capacitance step from one or more phosphorus related defects and one or more phosphorus independent defects.

Comparison of the introduction rates in float-zone diodes and Czochralski diodes confirms the dependence of the 70 °K (174 meV) defect on oxygen and indicates that the 203 °K (358 meV) defect is also oxygen related. The introduction rates of the other defects increase with decreasing oxygen concentration.

The results of the measurements to determine

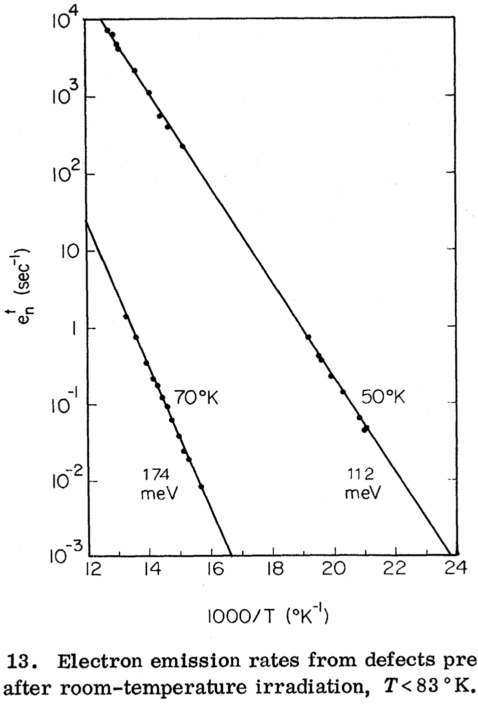

FIG. 13. Electron emission rates from defects present after room-temperature irradiation, $T < 83$ °K.

TABLE VI. Least-squares-fit parameters for different powers of T in the preexponential factor for electron traps present after room-temperature irradiation. Tolerances indicated are 70% fiducial limits: $e_n^t = A_n^t \times (\frac{1}{300}T)^m e^{-\Delta E/kT}$.

m	ΔE (meV)	A_n^t (10^{12} sec^{-1})
	$E_C - E_T = 112$ meV, $T_{1/2} = 50$ °K	
2	112.0 ± 0.4	1.57 ± 0.12
1	117.6 ± 0.4	0.946 ± 0.046
0	123.2 ± 0.4	0.571 ± 0.037
−1	128.8 ± 0.4	0.344 ± 0.023
	$E_C - E_T = 174$ meV, $T_{1/2} = 70$ °K	
2	174.2 ± 1.4	10.8 ± 2.5
1	180.2 ± 1.4	6.80 ± 1.6
0	186.1 ± 1.4	4.27 ± 0.97
−1	192.1 ± 1.4	2.67 ± 0.62
	$E_C - E_T = 236$ meV, $T_{1/2} = 104$ °K	
2	235.5 ± 0.6	0.281 ± 0.016
1	246.5 ± 0.5	0.333 ± 0.018
0	257.4 ± 0.6	0.395 ± 0.022
−1	268.3 ± 0.7	0.467 ± 0.031
	$E_C - E_T = 413$ meV, $T_{1/2} = 170$ °K	
2	412.8 ± 2.6	0.245 ± 0.042
1	427.8 ± 2.7	0.387 ± 0.068
0	442.8 ± 2.8	0.610 ± 0.111
−1	457.8 ± 2.9	0.963 ± 0.182
	$E_C - E_T = 471$ meV, $T_{1/2} = 175$ °K	
2	470.6 ± 1.5	7.63 ± 0.68
1	488.8 ± 1.3	14.9 ± 1.1
0	507.0 ± 1.1	29.1 ± 1.9
−1	525.2 ± 0.95	56.8 ± 3.3
	$E_C - E_T = 358$ meV, $T_{1/2} = 203$ °K	
2	358.2 ± 14.5	(7.2 ± 5.6) × 10^{-3}
1	376.8 ± 14.6	(1.41 ± 1.11) × 10^{-4}
0	395.4 ± 14.6	(2.76 ± 2.16) × 10^{-4}
−1	414.0 ± 14.6	(5.4 ± 4.2) × 10^{-4}

the defect properties after room-temperature irradiation are given in Table VIII.

IV. ANNEALING PROPERTIES OF DEFECTS

Further information on the nature of these defects can be obtained be determining their annealing characteristics and comparing with other published results. The diodes were isochronally annealed in a temperature-controlled chamber in a nitrogen atmosphere for periods of 30 min at 25 °C intervals. The temperature was maintained to ± 0.5 °C. After each anneal, TSCAP measurements were performed to monitor the changes in the deep-level inventory. Figure 14 illustrates a series of these measurements. (The curves are offset horizontally for clarity.) Changes in the deep-level inventory are evident by the appearance and disappearance of capacitance steps.

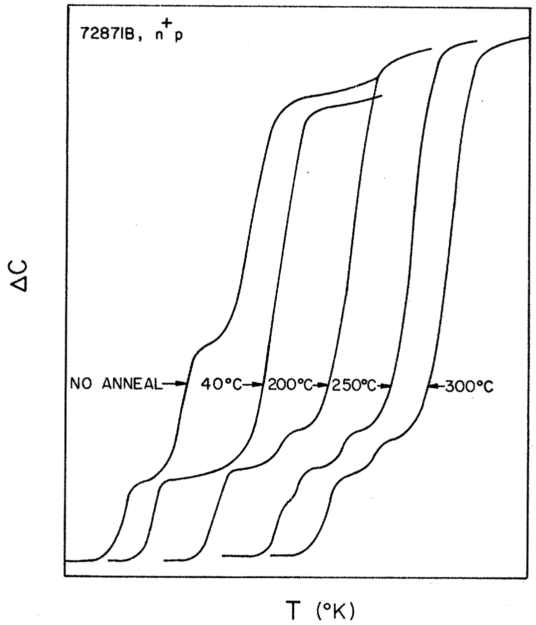

FIG. 14. TSCAP measurements on an annealed n^+p diode.

The results of the concentration measurements made after the anneal of n^+p diodes are plotted versus the annealing temperature in Fig. 15. The introduction of new defects after annealing at 175 and 225 °C is observed. The curves are marked with the activation energy determined from emission-rate measurements.

The annealing of the 291- and 354-meV defects shows interesting behavior. Room-temperature annealing of these defects is observed. The points marked with crosses in Fig. 15 are concentration

TABLE VII. Introduction rates of defects with energy levels above midgap measured in p^+n diodes with different substrate phosphorus and oxygen concentrations.

		$T_{1/2}$ (°K) [ΔE (meV)]				
N_{phos} (cm^{-3})	Type	50 [112]	70 [174]	104 [236]	175 [413; 471]	203 [358]
6.7×10^{13}	Czochralski	trace	0.219	0.0061	0.0071	0.0006
5.1×10^{14}	Czochralski	trace	0.220	0.0069	0.0069	0.0006
5.3×10^{15}	Czochralski	trace	0.225	0.0059	0.015	0.0009
8.7×10^{13}	float zone	0.300	0.012	0.012	0.270	0

TABLE VIII. Results of measurements after room-temperature irradiation.

ΔE (meV)	Impurity dependences determined
$E_C - E_T = 123$	undetermined
186	oxygen dependent, phosphorus independent
257	oxygen and phosphorus independent
443	phosphorus independent
507	phosphorus dependent, oxygen independent
$E_T - E_V = 386$	boron independent
317	boron independent
207	boron independent

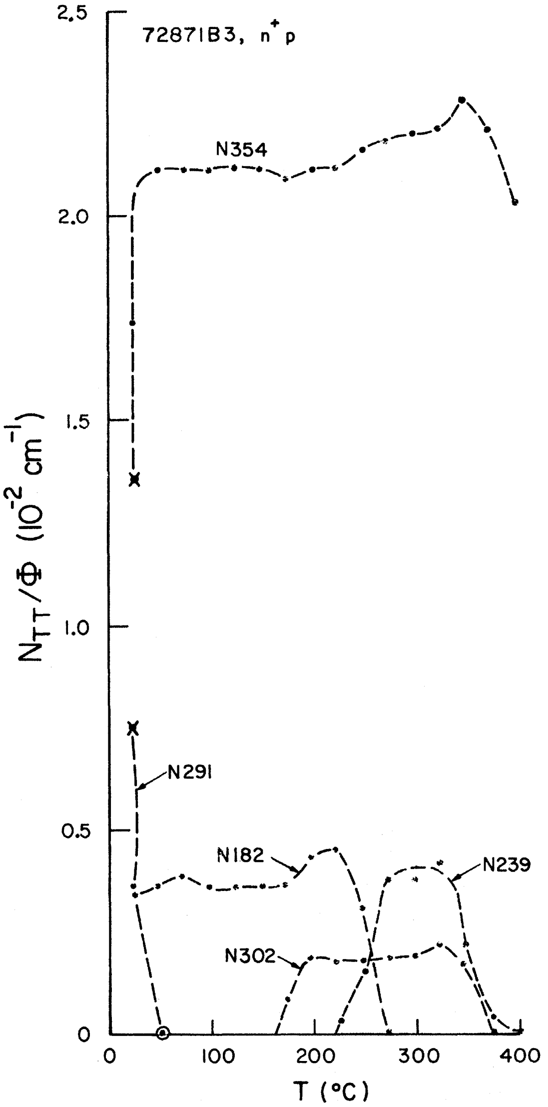

FIG. 15. Annealing behavior of defect concentrations in an n^+p diode.

measurements made shortly after irradiation. The second point at 25 °C is the defect concentration after a 30-min room-temperature anneal. A decrease in the concentration of the 291-meV defects is accompanied by an identical increase in the 354-meV concentration, indicating that one defect is being converted into the other by room-temperature annealing. (A long irradiation at high flux could result in the 291-meV defect not being observed at all, due to sample heating.)

Only the 354-meV defect survives 400 °C annealing. The annealing was terminated at this temperature due to diode deterioration near the gold-silicon eutectic.

The results of the annealing of p^+n diodes are given in Fig. 16. The curves show the introduction of a new defect in Czochralski diodes at 350 °C, yield confirmation of the two-defect nature of the 175 °K capacitance step, correlate the phosphorus-vacancy defect with the 471-meV thermal-activation energy, and correlate the oxygen-vacancy defect with the 174-meV thermal-activation energy.

The annealing of the 175 °K capacitance step in the high-phosphorus Czochralski diodes and in the float-zone diodes shows an annealing stage at 100–150 °C that is not observed in the low-phosphorus Czochralski diodes. This annealing stage has been correlated with the phosphorus-vacancy defect.[42,43] The 175 °K capacitance step is therefore composed of the phosphorus-vacancy pair and a second phosphorus-independent defect of unknown nature.

The oxygen-vacancy pair has been shown to anneal at 300–350 °C.[24,44,45] In Fig. 16, the 70 °K defect, already shown to be oxygen related, is shown to anneal in this temperature range. This correlates the 174-meV emission activation energy with the oxygen-vacancy pair.

Consider now the annealing above 150 °C related to the 175 and 104 °K capacitance steps in the Czochralski diodes. The annealing of these two steps is almost identical for both phosphorus concentrations in the 150–250 °C range. Above 250 °C, the curves separate into pairs associated with the two phosphorus concentrations. This behavior suggests that the 236- and 413-meV thermal-activation

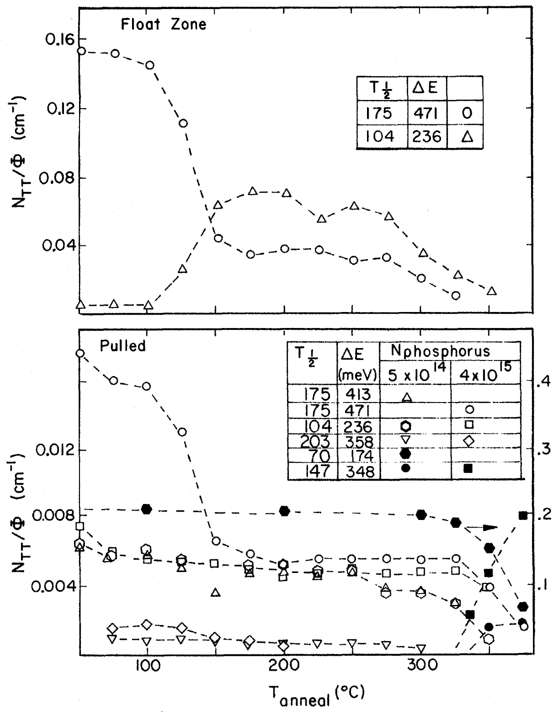

FIG. 16. Annealing behavior of defect concentrations in p^+n diodes.

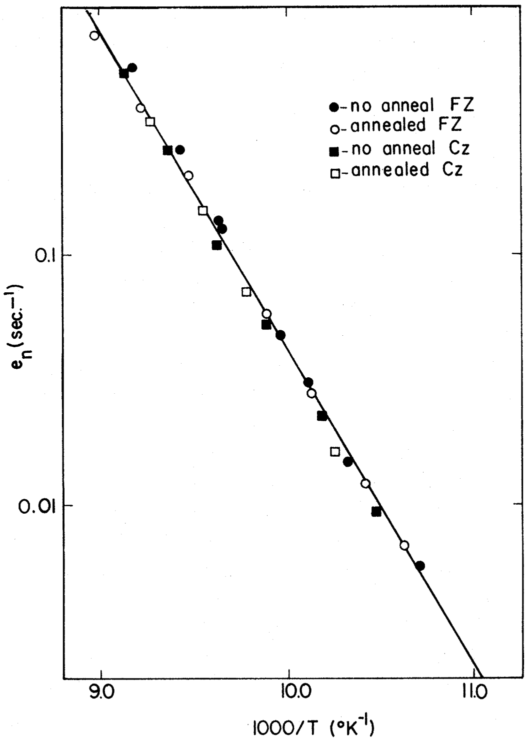

FIG. 17. Electron emission rates related to 104 °K capacitance step in annealed and unannealed Czochralski and float-zone diodes.

energies are associated with the same defect center, the defect annealing temperature being dependent on the phosphorus concentration. This type of annealing behavior has been observed[46,47] for the phosphorus-vacancy center and attributed to charge-state effects[47] or to interactions between defects.[48]

The annealing of the two capacitance steps in float-zone material does not allow this conclusion, however. Though the annealing of the 175 °K step in float-zone material is qualitatively similar to the annealing of this step in Czochralski material, the annealing of the 104 °K capacitance step shows negative annealing (apparently associated with the annealing of the phosphorus-vacancy pair) and the introduction rates are not equal in the range of 150–250 °C.

The relationship between 175 and 104 °K defects is, therefore, not clear from these annealing measurements. It is not clear that the defects observed in Czochralski material are the same as those observed in float-zone material, nor how the defects present after room-temperature irradiation are related to those present after annealing at 200 °C. To obtain further information to answer these questions, the emission rates related to the 104 and 175 °K capacitance steps were measured and compared for Czochralski and float-zone material after room-temperature irradiation and after the 200 °C anneal. The emission rates measured under these four conditions could indicate differences in the defects present.

The results of these measurements related to the 104 °K capacitance step are indicated in Fig. 17. No significant difference is observed in the four emission-rate measurements, implying that the defect observed in Czochralski material is the same as that observed in float-zone material and that this defect survives 200 °C annealing.

The results of these measurements, related to the 175 °K capacitance step, are presented in Fig. 18 and indicate the complex nature of the associated defects. Six different sets of measurements are shown, since a difference between Czochralski diodes with varying phosphorus concentrations has already been observed. The data can be fitted to four different slopes. The solid line is the same as the 471-meV curve in Fig. 12. It is measured in unannealed float-zone diodes and high-phosphorus-concentration Czochralski diodes and is related to the phosphorus-vacancy pair. The dash-cross line was measured on float-zone diodes after annealing out the phosphorus-vacancy pair. The dash line was measured in low-phosphorus Czochralski diodes before and after annealing. The emis-

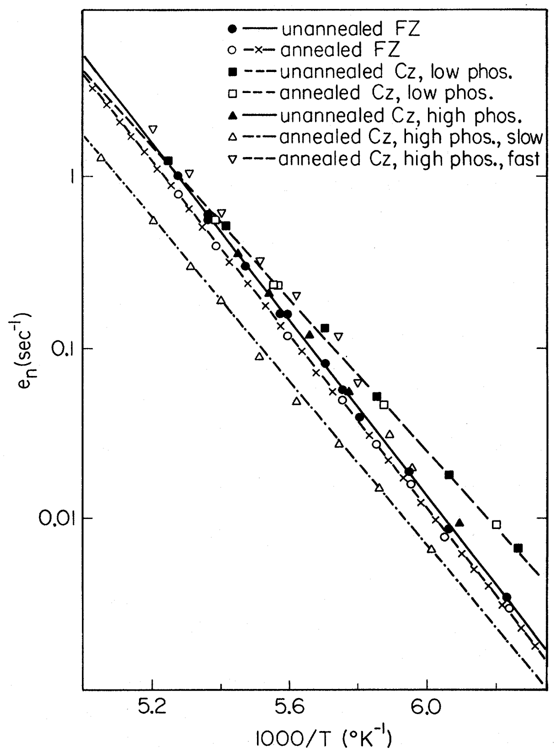

FIG. 18. Electron emission rates related to 175 °K capacitance step in annealed and unannealed Czochralski and float-zone diodes.

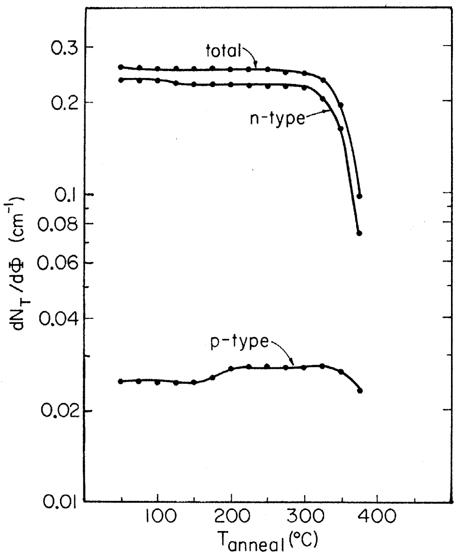

FIG. 19. Annealing behavior of total defect concentration in Czochralski diodes.

sion-rate measurements after annealing the high-phosphorus Czochralski diodes showed nonexponential transients. It was found that this could be fitted to two exponentials, indicating the presence of two defects. The fast component of this decay coincided with the emission rates measured in low-phosphorus Czochralski diodes (dash line). The slow component introduced the fourth slope (dash-dot line).

These data indicate that as many as four different defects may be contributing to the 175 °K capacitance step, all with thermal-emission activation energies between 413 and 471 meV. It has been known for some time that several different defects give energy levels in this range (see Ref. 43, pp. 84–86).

The emission rates measured in annealed (dash-cross line) and unannealed (solid line) float-zone material are similar, having approximately the same slope but a slightly smaller magnitude. One may speculate that this means that the defects observed in annealed float-zone material are stabilized phosphorus-vacancy pairs. These stabilized pairs would not be seen in Czochralski diodes because of the large concentration of 413-meV defects.

The annealing behavior of the total defect concentration in Czochralski material is shown in Fig. 19. The introduction rates in Figs. 15 and 16 were added to obtain the curves labeled p-type and n-type, respectively. These were then added to give the total defect concentration. The shape of this curve is dominated by annealing of the oxygen-vacancy pair. Though the impurities in the n- and p-type samples differ, the shape of these curves is not affected, since no impurity dependences were observed for the impurity concentration in these samples (5×10^{14} cm^{-3}).

V. DEFECTS INTRODUCED BY ANNEALING

The impurity dependence of the defects introduced by annealing was investigated by measuring their introduction rates in diodes with varying doping impurity concentrations. In Fig. 16, the level introduced at 350 °C is represented by solid circles for a phosphorus concentration of 5×10^{14} cm^{-3} and by solid squares for 4×10^{15} cm^{-3}. The introduction rate is seen to increase with phosphorus concentration, implying that this defect is phosphorus related. Since it appears to be related to the oxygen-vacancy annealing, it may also be oxygen related. The oxygen-vacancy pair moving through the lattice may be trapped and stabilized at a phosphorus site to form a phosphorus-oxygen-vacancy defect. It is possible also that the oxygen-vacancy pair breaks up and only one of the constituents is trapped at the phosphorus site. Similar possibilities have been discussed by Corbett *et al.*[45]

The impurity dependence of the defects introduced in p-type silicon was determined in a similar fashion. The introduction rates for samples with different boron concentrations are shown in Fig. 20 versus annealing temperature. The introduction rates are independent of the boron concentration implying that these defects are not boron-defect complexes.

The activation energies related to these defects were determined from emission rate versus temperature measurements. The results appear in Fig. 21. The data were least-squares fitted to Eq.

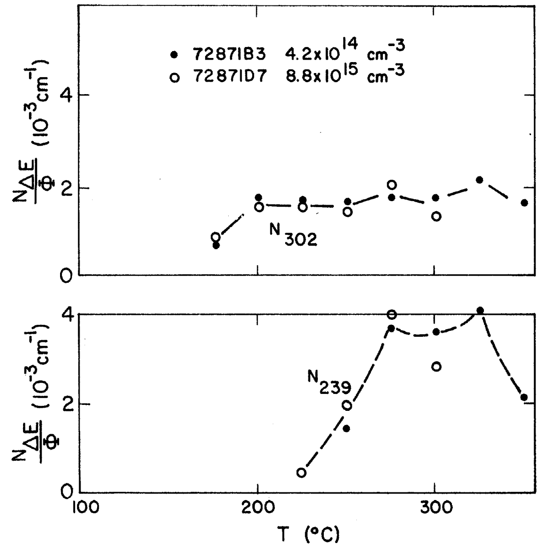

FIG. 20. Boron dependence of introduction rates of defects produced by annealing.

TABLE IX. Least-squares-fit parameters for different powers of T in the preexponential factor for annealed-in defects. Tolerances indicated are 70% fiducial limits: $e^t_{n,p}=A^t_{n,p}(\frac{1}{300}\,T)^m e^{-\Delta E/kT}$.

m	ΔE (meV)	$A^t_{n,p}$ (10^{12} sec^{-1})
	$E_C-E_T=348$ meV, $T_{1/2}=147$ °K	
2	347.7 ± 6.9	0.303 ± 0.169
1	360.3 ± 6.9	0.402 ± 0.222
0	372.9 ± 7.0	0.534 ± 0.295
−1	385.6 ± 7.0	0.708 ± 0.392
	$E_V-E_T=302$ meV, $T_{1/2}=120$ °K	
2	301.5 ± 0.7	3.37 ± 0.19
1	314.7 ± 0.7	4.78 ± 0.25
0	327.8 ± 0.7	6.78 ± 0.38
−1	340.9 ± 0.8	9.62 ± 0.63
	$E_V-E_T=239$ meV, $T_{1/2}=99$ °K	
2	238.8 ± 0.7	1.38 ± 0.10
1	249.4 ± 0.6	1.58 ± 0.11
0	259.9 ± 0.6	1.80 ± 0.12
−1	270.5 ± 0.7	2.05 ± 0.15
	$E_C-E_T=458$ meV, $T_{1/2}=176$ °K	
2	458.4 ± 1.2	2.82 ± 0.19
1	476.6 ± 1.2	5.50 ± 0.37
0	494.7 ± 1.2	10.7 ± 0.75
−1	512.9 ± 1.3	20.9 ± 1.6
	$E_C-E_T=442$ meV, $T_{1/2}=179$ °K	
2	442.0 ± 7.2	0.505 ± 0.234
1	457.4 ± 7.2	0.819 ± 0.384
0	472.8 ± 7.3	1.33 ± 0.63
−1	408.2 ± 7.4	2.15 ± 1.0

(8) with the results as given in Table IX. Data from Fig. 18 are also included in Table IX.

VI. CHARGE-STATE DETERMINATION

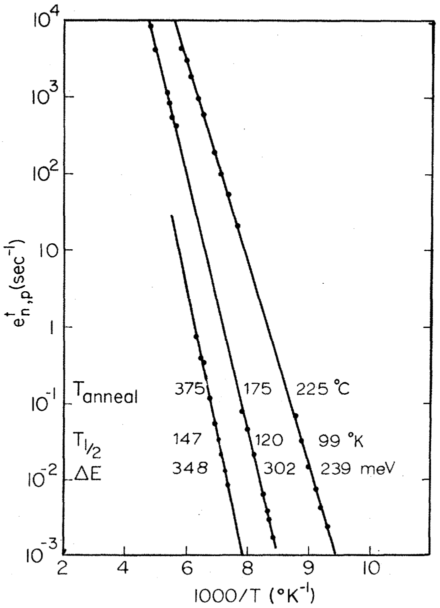

FIG. 21. Majority carrier emission rates of defects produced by annealing.

The charge state of the defects produced by electron irradiation can be determined by measuring the charge they introduce in the depletion region of a reverse-biased diode. The charge concentration before irradiation (corresponding to the shallow-level doping impurity concentration) is measured and analyzed by Eq. (4) and compared to the concentration after irradiation (corresponding to the net concentration resulting from the doping impurities and the charged defects). Differences in these two quantities are compared with defect concentrations to determine the charge of individual defects.

At room temperature, the emission rates will be large and steady-state charge state may be assumed immediately (no electrons trapped at levels in the upper band gap, no holes trapped at levels in the lower band gap). The effect on the charge concentration of various kinds of defects is given in Table X. The total change in the impurity concentration due to irradiation will be given by the net effects of the various types of defects introduced.

The results of these charge concentration measurements are given in Table XI. For Czochralski

TABLE X. Changes in the magnitude of the charge concentration in the depletion region of a reverse-biased diode due to the introduction of various types of defects: ρ(after irradiation) = ρ(before irradiation) + $q\Delta$.

	Δ			
	Defects below midgap, $e_p > e_n$		Defects above midgap, $e_n > e_p$	
Defect type	p-type	n-type	p-type	n-type
single acceptor	$+N_{TT}$	$-N_{TT}$	0	0
single donor	0	0	$-N_{TT}$	$+N_{TT}$
single acceptor-like one impurity complex	0	$-2N_{TT}$	$-N_{TT}$	$-N_{TT}$
single donor-like one impurity complex	$-N_{TT}$	$-N_{TT}$	$-2N_{TT}$	0

TABLE XI. Charge concentration measurement results: p (after irradiation) $= p$ (before irradiation) $+ q\Delta$.

Type	Δ	Annealing
p type (Czochralski)	0	no correlations
n type (Czochralski)	0	no correlations
n type (Float zone)	$\simeq -N_{507}(PV)$	$\Delta \rightarrow 0$ as PV anneals

material, no significant change is observed after irradiation or during annealing in either p type or n type. This information, together with the lack of impurity dependences, was compared to Table X. It implies that the defects above midgap are acceptors and those below midgap are donors.

For float-zone material, changes in the charge concentration were observed that correlated in magnitude with the concentration of the phosphorus-vacancy pair. This change annealed out during the annealing stage associated with the phosphorus vacancy. This follows the behavior indicated in Table X for a single-acceptor-like one-impurity complex with energy level above midgap.

The validity of these measurements for the case of the defects in n-type Czochralski with small defect concentrations is questionable. The concentrations of these defects were never more than a few percent of the impurity concentration. Changes in the total charge magnitude of only a few percent were not deemed significant.

VII. COMPARISON WITH PREVIOUSLY PUBLISHED WORKS

Tables XII and XIII summarize the properties of defects introduced in silicon by 1.0-MeV electron irradiation as determined by these measurements. These results can be compared with those obtained using other methods. Before this comparison is made, it would be useful to discuss the question of whether the measurement techniques used in this study introduce effects not seen in other bulk measurements. In the studies reported here, a limited region of the silicon crystal is investigated. This region lies within 10–30 μ of a diffused pn junction or a Schottky barrier. The diffused region, 3–5 μ deep, contains a high concentration of impurities. In most other studies, the sample has a uniform impurity concentration.

In the diodes used in these studies, the concentration of impurities in the diffused region is 10^4 to 10^5 times the concentration in the substrate. A consequence of this is that the depletion region lies mostly on the lowly doped side of the junction. Therefore, the defects observed in these studies are located in the substrate of the diode and not in

TABLE XII. Summary of results for defects observed in n-type silicon.

ΔE(meV)	N_{TT}/Φ (cm^{-1}) Czochralski	Float zone	Charge state	Impurity dependence Oxygen	Phosphorus	A_n(10^{12} sec^{-1})	$T_{1/2}$ (°K) $b = 0.4$ °K/sec	Annealing In °C	Out °C	References reporting similar energies or behavior
112	⋯	0.300		no		1.57	50			3, 10, 12, 51
174	0.221	0.012	acceptor	yes	no	10.8	70		350	1, 2, 5, 8, 10, 12–16, 19, 23–25, 42, 44, 51
236	0.006	0.012	acceptor	no	no	0.281	104		325	5, 14, 19, 21
348	0	0			yes	0.303	147	325		45, 52
413	0.007 0.001	0			no	0.245	172		325	2–6, 8, 16, 21, 23, 25, 26, 42, 47, 51, 53
442	0	0			yes	0.505	179		350	
471	0.014	0.270	acceptor	no	yes	7.63	175		125	
458	0	0		no		2.82	176	150	350	
358	0.0006	0		yes	no	0.0072	203		200	

TABLE XIII. Summary of results for defects observed in p-type silicon.

						Annealing		
ΔE(meV)	N_{TT}/Φ (cm^{-1})	Charge state	Boron dependence	A_p(10^{12} sec^{-1})	$T_{1/2}$ (°K) $b = 0.4$ °K/sec	In °C	Out °C	References reporting similar energies or behavior
182	0.004	donor	no	0.0599	89		250	4, 5, 7, 9, 15, 17, 20, 28
239	0	donor	no	1.38	99	175	350	
291	see text	donor	no	1.30	119		25	4, 20
302	0	donor	no	3.37	120	225	350	
354	0.025	donor	no	0.237	150	25		7, 11, 14, 21–23, 28

the diffused region with its high impurity concentration. Defects in the highly doped region make no contribution to the observed capacitance transients. This is verified by the fact that the capacitance steps observed in one diode polarity are not observed in the other.

An electric field is present in a portion of the diode even at zero bias due to the built-in potential. However, as shown in Fig. 2, the defects lying in this region do not contribute to the capacitance transients. During irradiation and annealing, the diode was zero biased so that the measured introduction and annealing rates were not affected by an electric field.

Although the defects observed in this work are located in the region of lower impurity concentration, the presence of the nearby high-impurity region could influence the measurement results if this region acted as a sink or source of defects during the irradiation or annealing. This possibility was investigated by measuring the spatial variation of the defect concentration, using differential capacitance measurements.[40] These measurements were made twice, once with the defects charged and once with the defects neutral. The difference between these two measurements gives the spatial variation of the defect concentration. If the diffused region acts as a sink (or source), it would be expected that the defect concentration near the junction would be larger (smaller) than the concentration farther from the junction. Typical results of the concentration-profile measurements are given in Fig. 22, for both diode polarities. It is seen that the defect concentration is virtually constant, indicating that the diffused region is not a source or sink of defects.

The conclusion to be reached from these considerations is that the impurity profile present in the diodes of this study introduces no effects that would not be expected in uniform bulk measurements. The thermal-emission activation energies reported here may not be directly comparable to other energy-level measurements, however. The thermal-emission activation energy is defined by Eq. (8). Each value of m in this equation defines a different thermal-activation energy. Tables IV, VI, and IX indicate that the experimental data are fitted with the same percentage uncertainty by several values of m. Therefore, the "correct" choice of m cannot be determined from experiment. Although for a given m, the experimental data yield a highly accurate energy, the uncertainty introduced by the choice of m is of the order of ± 10%.

The thermal-emission activation energies quoted in the text are obtained using $m = 2$ in Eq. (8). This value was chosen as the most plausible value by considering detailed balance at thermal equilibrium. This principle relates the emission rate to the capture cross section:

$$e^t_{n(p)} = v_{\text{th}} \sigma^t_{n(p)} N_{C(V)} e^{-\Delta E/kT}, \tag{9}$$

where v_{th} is the average thermal velocity, $\sigma^t_{n(p)}$ is the electron-(hole-) capture cross section, and

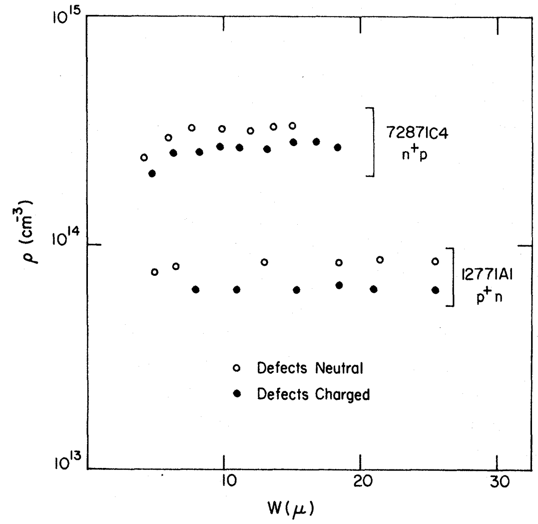

FIG. 22. Spatial variation of the defect concentration in n^+p and p^+n diodes.

TABLE XIV. Comparison of results of Sonder and Templeton[5,7] (ST) with the results of this study.

ΔE(meV)		
ST	This work	Comments
not observed	E_C-112	
E_C-170	174	only level ST observed in n-type Czochralski
E_C-210	236	observed by ST after annealing to 280 °C
not observed	373	
E_C-470	413 442 458 471	ST observed annealing at 100–150 °C with a residual concentration not annealable at 280 °C
not observed	358	
E_V+350	E_V+354	ST observed annealing at 350 °C
not observed	302	
not observed	291	
not observed	239	
E_V+210	182	ST observed this level in float-zone material, but not in Czochralski material; annealing was observed at 180–200 °C

$N_{C(V)}$ is the effective density of states in the conduction (valence) bond. The value of m may be inferred from the temperature dependence of the preexponential factor in Eq. (9). The temperature dependence of the cross section must be known. For all of the defects in this study, the measured emission rate corresponds to a transition from a charge state to a neutral state. The inverse process of capture then corresponds to capture by a *neutral* defect. Measurements of capture cross sections of neutral defects generally show no temperature dependence.[54,55] Then, with $v_{\text{th}} \sim T^{1/2}$, $N \sim T^{3/2}$, and $\sigma^t \sim T^0$, Eq. (9) gives

$$e^t_{n(p)} \sim T^2 e^{-\Delta E/kT}. \qquad (10)$$

Thus, $m=2$ is a plausible choice, assuming that Eq. (9) is accurate when high fields are present and that neutral centers are involved. For the case of charged defects, when excited states may play an important role in the emission process, an analysis by Ning[56] indicates that $m=0$ is the proper choice.

Because of this uncertainty in the choice for m, comparison of the thermal-emission activation energies reported here, with energy-level measurements reported using other techniques, must be approximate. Defect correlations must be made through observed impurity dependences, annealing behavior, and approximate energy-level agreement. The results of other measurements will now be compared to the results reported here, with this limitation in mind.

A. Other Defect Inventory Measurements

The results of other measurements are summarized in Table I. Comparison with Tables XII and XIII shows that the activation energies observed in these studies are similar to those observed earlier. This is the first work in which these levels are observed simultaneously.

A study that closely parallels that described here has been published by Sonder and Templeton[5,7] (ST), who used Hall-effect measurements to investigate the energy levels appearing in silicon subjected to ^{60}Co γ irradiation. Their results are compared to those of this study in Table XIV.

The defects observed by ST correspond to the defects having the largest concentrations. The defects with smaller concentrations were not measured, although ST made several references to slight changes in the Hall coefficient that could not be resolved. Several of these defects were observed only in float-zone material when the dominant E_C-174-meV or E_V+354-meV defects were absent, whereas the defects were observable in both Czochralski and float-zone materials in this study.

ST report one level not observed here. This was a level at E_V+280 meV observed only in float-zone p-type material, which was not studied in these measurements.

The annealing behavior reported by ST for their E_C-210 meV, E_V+350 meV, and E_V+210 meV is very similar to the annealing behavior of the E_C-236-meV, E_V+354-meV, and E_V+182-meV centers reported here. They failed to observe the room-temperature annealing of the 291-meV defect and to analyze the levels introduced by annealing.

Another study reporting similar energy levels is one by Almeleh and Goldstein.[28] They report levels in p-type silicon at E_V+390 meV, E_V+300 meV, and E_V+200 meV. Although there are other similarities between the two sets of data, Almeleh and Goldstein conclude quite different characteristics for the defects they observed. Their results will be discussed further in the section on spin-resonance measurements (Sec. VIIB).

B. Spin-Resonance Measurements

Comparisons with spin-resonance measurements[24–28] has allowed the identification of two of the defects observed. The phosphorus-vacancy pair is associated with the 471-meV activation energy and the oxygen-vacancy pair is associated with the 174-meV energy. These identifications are made through the observed impurity dependences and annealing behavior.

There are other reported spectra that may be related to defects observed here. Jung and Newell,[57] studying neturon-irradiation silicon, observed annealing behavior very similar to that reported here; defects annealing in and out, in the range 100–500 °C. Though the shapes of several of their curves match those here, there is poor agreement in the annealing temperatures. The only reasonable correlation occurs between their Si-*N* center and the $E_V + 302$-meV center. Though different defects may be introduced by neutron irradiation, it is of interest to look for these correlations.

Daly[58] has reported a center (Si*B*3) in neutron-irradiated silicon that has similar annealing behavior to the $E_V + 239$-meV center.

Almeleh and Goldstein[28] have studied paramagnetic defects in *p*-type silicon. The energy levels they observed were discussed in Sec. VII A. They observe the *K* center (Si*G*15) in Czochralski material, the *J* center (Si*G*6) in float-zone material. There are two correlations between their measurements of the *K* center and the $E_V + 291$-meV center observed here: (i) The energy level determined from Hall-effect measurements was 300 meV; (ii) the defect was not observed after heavy bombardment. The 291-meV defect is not observed after heavy irradiation due to annealing caused by heating effects.

Almeleh and Goldstein found, however, that the defect can be observed under illumination or after 300 °C annealing and attribute the loss of the resonance to depopulation of the level, rather than annealing. It is interesting to note that the $E_V + 302$-meV defect is introduced by 300 °C annealing and that the associated emission rates are very similar to the 291-meV rates. It would be difficult to understand, however, how a defect unstable at room temperature could reappear after 300 °C annealing, suggesting that these are two different centers. Carter[59] has measured properties of a defect with 300-meV energy level, stable to 400 °C that is a more likely candidate for the *K* center.

Almeleh and Goldstein report a deeper level at $E_V + 390$ meV that is responsible for the hole depopulation of the *K* center. This center must anneal at $T < 300$ °C to explain the reappearance of the *K*-center spectra. A center at $E_V + 354$ meV is reported here but is stable to above 400 °C.

Almeleh and Goldstein associated the *J* center with a level at $E_V + 200$ meV, similar to the 182-meV center observed here. The *J* center, however, has been associated with the divacancy[27] which anneals at 300 °C.[27] The 182-meV center anneals at 225 °C.

There have been other spectra detected[60] for which only the *g* values have been reported. Some of these spectra may be related to defects reported here, but this cannot be determined until the impurity dependence and annealing behavior of the spectra are reported.

C. Annealing Measurements

The annealing measurements reported here were important in identifying the oxygen-vacancy pair and the phosphorus-vacancy pair. They also established the complex nature of the defects with energies between 413 and 471 meV. Annealing measurements made by other investigators are useful to compare their results with those reported here.

(i) Room-temperature annealing has been observed by Malovetskaya[4] and Vavilov.[20] The energy level was located at $E_V + 210$ meV or $E_V + 250$ meV.

(ii) Sonder and Templeton[7] have observed annealing of an $E_V + 210$-meV defect at 180–200 °C and annealing of an $E_V + 350$-meV defect at 350 °C in good agreement with the annealing behavior of the 182- and 354-meV centers observed here.

(iii) The introduction of defects by annealing has been observed many times.[9,45,57] This is probably related to the negative annealing often observed.[17,51,52,61] The defects introduced in *p*-type silicon may be related to those observed by Jung and Newell[57] and by Daly.[58] The defect introduced at 325 °C associated with the oxygen-vacancy anneal may be the same as that observed by Corbett *et al.*[45] and by Tauke and Faraday.[52]

Figure 19 gives evidence that these defects introduced by annealing are the result of reordering of electrically active defects already present. In this figure, it is seen that the total defect concentration is almost constant until the oxygen vacancy begins to anneal around 300 °C. Inuishi and Matsuura[14] have suggested that reverse annealing of lifetime at an annealing temperature around 200 °C is related to dissociation of the oxygen-vacancy pair. This suggestion is consistent with our measurements since new defects are introduced at this temperature and a slight decrease in the oxygen-vacancy concentration is observed.

The annealing of the phosphorus-vacancy pair is accomplished by the dissociation of the components. This can be seen by the fact that measurements of the room-temperature charge concentration in the depletion region made after each anneal show that the phosphorus atoms are returning to their shallow-level configuration. The negative annealing of the 236-meV center observed in Fig. 16 is probably associated with the capture of the free vacancy by some other defect.

D. Defects Not Observed in This Work

Several defects commonly observed in silicon were not detected in these measurements. These were the divacancy,[21,25,27,62–64] a boron complex,[20,22] and a stable defect with an energy level about 300 meV above the valence band.[1,2,6,8,28,65]

The divacancy introduces three energy levels in the band gap at $E_C - E_T = 0.4$ eV,[21] $E_C - E_T = 0.54$ eV,[21] and $E_T - E_V = 0.27$ eV,[25] and anneals at 300 °C.[27] The presence of the divacancy would be detected in these measurements by observing three activation energies with identical introduction rates and annealing behavior. This was not observed. In addition, a defect with a midgap level should dominate the reverse current temperature behavior.[50] Measurements[54] of the temperature dependence of the leakage current yielded an activation energy of 780 meV, indicating it is associated with the 354-meV defect, rather than a midgap level. It is suggested that the divacancy concentration is too small to be detected in this work placing an upper limit on its introduction rate in these samples of 0.0001 cm^{-1}.

The acceptor-defect complexes identified by Cherki and Kalma[22] were observed in samples with higher doping subjected to larger doses than the samples in this study. This may explain why they were not observed in this work.

The defect with a level 300 meV above the valence band has already been discussed relative to the Almeleh–Goldstein measurements of the *K* center. This level has been observed using Hall-effect measurements and lifetime measurements. It is possible that this defect is the same as the 354-meV defect observed here; the annealing behavior[4,59] is similar. It is also possible that some of the lifetime measurements are detecting the 236-meV defect observed in the upper band gap. The level has been observed by Wilson,[65] in neutron-irradiated silicon using similar capacitance measurements.

---

*Work supported in part by the Advanced Research Projects Agency the National Science Foundation (GH-33634) and the Air Force Office of Scientific Research (AFOSR-71-2067). Based on the doctoral thesis in physics of JWW.

†Present address: Texas Instruments, Inc. Dallas, Tex.

[1] G. K. Wertheim, Phys. Rev. **110**, 1272 (1958).

[2] D. E. Hill, Phys. Rev. **114**, 1414 (1959).

[3] G. K. Wertheim and D. N. E. Buchanan, J. Appl. Phys. **30**, 1232 (1959).

[4] V. M. Malovetskaya, G. N. Galkin, and V. S. Vavilov, Fiz. Tverd. Tela **4**, 1372 (1962) [Sov. Phys.-Solid State **4**, 1008 (1962)].

[5] E. Sonder and L. C. Templeton, J. Appl. Phys. **34**, 3295 (1963).

[6] T. Tanaka and Y. Inuishi, Jap. J. Appl. Phys. **4**, 725 (1965).

[7] E. Sonder and L. C. Templeton, J. Appl. Phys. **36**, 1811 (1965).

[8] J. R. Carter, Jr., J. Phys. Chem. Solids **27**, 913 (1966).

[9] H. Djerassi, J. Merlo-Flores, and J. Messier, J. Appl. Phys. **37**, 4510 (1966).

[10] H. J. Stein and F. L. Vook, Phys. Rev. **163**, 790 (1967).

[11] I. D. Konozenko, A. K. Semencyuk, and V. I. Khrivich, Phys. Status Solidi **35**, 1043 (1969).

[12] A. Vapaille, Ann. Phys. (Paris) **3**, 5 (1968).

[13] G. N. Galkin, N. S. Rytova, and V. S. Vavilov, Fiz. Tverd. Tela **2**, 2025 (1960) [Sov. Phys.-Solid State **2**, 1819 (1961)].

[14] Y. Inuishi and K. Matsuura, J. Phys. Soc. Jap. Suppl. **18**, 240 (1963).

[15] J. A. Baicker, Phys. Rev. **129**, 1174 (1963).

[16] R. H. Glaenzer and C. J. Wolf, J. Appl. Phys. **36**, 2197 (1965).

[17] T. Nakano, K. Nakasima, and Y. Inuishi, J. Phys. Soc. Jap. **20**, 2140 (1965).

[18] M. Hirata, M. Hirata, and H. Saito, J. Appl. Phys. **37**, 1867 (1966).

[19] H. Y. Fan and A. K. Ramdas, J. Appl. Phys. **30**, 1127 (1959).

[20] V. S. Vavilov, A. F. Plotnikov, and V. D. Tkachev, Fiz. Tverd. Tela **4**, 3446 (1962) [Sov. Phys. Solid State **4**, 2522 (1963)].

[21] A. H. Kalma and J. C. Corelli, Phys. Rev. **173**, 734 (1968).

[22] M. Cherki and A. H. Kalma, Phys. Rev. B **1**, 647 (1970).

[23] R. C. Young and J. C. Corelli, Phys. Rev. B **5**, 1455 (1972).

[24] G. Bemski, J. Appl. Phys. **30**, 1195 (1959).

[25] G. D. Watkins and J. W. Corbett, Discuss. Faraday Soc. **31**, 86 (1961).

[26] G. D. Watkins and J. W. Corbett, Phys. Rev. **134**, A1359 (1964).

[27] G. D. Watkins and J. W. Corbett, Phys. Rev. 138, A543 (1965).

[28] N. Almeleh and B. Goldstein, Phys. Rev. **149**, 687 (1966).

[29] C. T. Sah, W. W. Chan, H. S. Fu, J. W. Walker, Appl. Phys. Lett. **20**, 193 (1972).

[30] M. G. Buehler, Solid-State Electron. **15**, 69 (1972).

[31] C. T. Sah, L. Forbes, L. L. Rosier, and A. F. Tasch, Jr., Solid-State Electron. **13**, 759 (1970).

[32] J. W. Walker and C. T. Sah, Phys. Status Solidi A **11**, 513 (1972).

[33] For these measurements, "deep level" means an energy level with a depth in the gap greater than the depth of the energy level of the majority doping impurity.

[34] W. Shockley and W. T. Read, Jr., Phys. Rev. **87**, 835 (1952); R. N. Hall, Phys. Rev. **87**, 387 (1952).

[35] C. T. Sah, L. Forbes, L. L. Rosier, A. F. Tasch, Jr., and A. B. Tole, Appl. Phys. Lett. **15**, 145 (1969).

[36] L. L. Rosier and C. T. Sah, Solid-State Electron. **14**, 41 (1971).

[37] L. D. Yau and C. T. Sah, Phys. Status Solidi A6, 561 (1971).

[38] W. W. Chan and C. T. Sah, J. Appl. Phys. **42**, 4768 (1971).

[39] C. T. Sah, T. H. Ning, L. L. Rosier, and L. Forbes, Solid State Commun. **9**, 917 (1971).

[40] See, for example, S. M. Sze, *Physics of Semiconductor Devices* (Interscience, New York, 1969), p. 90.

[41] C. T. Sah, L. L. Rosier, and L. Forbes, Appl. Phys. Lett. **15**, 161 (1969).

[42] H. Saito and M. Hirata, Jap. J. Appl. Phys. **2**, 678 (1963).

[43] J. W. Corbett, *Electron Radiation Damage in Semiconductors and Metals* (Academic, New York, 1966), p. 77.

[44] J. W. Corbett, G. D. Watkins, R. M. Chrenko, and R. S. McDonald, Phys. Rev. **121**, 1015 (1961).

[45] J. W. Corbett, G. D. Watkins, and R. S. McDonald, Phys. Rev. **135**, A1381 (1964).

[46] P. H. Fang and P. Iles, Appl. Phys. Lett. **14**, 131 (1969).

[47] L. C. Kimerling, H. M. DeAngelis, and C. P. Carnes, Phys. Rev. B 3, 427 (1971).

[48] P. H. Fang and T. Tanaka, J. Appl. Phys. **42**, 5333 (1971).

[49] C. T. Sah and J. W. Walker, Appl. Phys. Lett. 22, 384 (1973).

[50] C. T. Sah, R. N. Noyce, and W. Shockley, Proc. IEEE **45**, 1228 (1957).

[51] K. Matsuura and Y. Inuishi, J. Phys. Soc. Jap. **16**, 1485 (1961).

[52] R. V. Tauke and B. J. Faraday, J. Appl. Phys. **37**, 5009 (1967).

[53] T. Tanaka and Y. Inuishi, J. Phys. Soc. Japan **19**, 167 (1964).

[54] J. W. Walker and C. T. Sah, Radiation Effects Journal (to be published).

[55] V. L. Bonch-Bruereich and E. G. Landsberg, Phys. Status Solidi **29**, 9 (1968), Table IV.

[56] T. H. Ning, Ph.D thesis (University of Illinois, 1970) (unpublished).

[57] W. Jung and G. S. Newell, Phys. Rev. **132**, 648 (1963).

[58] D. F. Daly, J. Appl. Phys. **42**, 864 (1971).

[59] J. R. Carter, Jr., IEEE Trans. Nucl. Sci. **13**, 24 (1966).

[60] See Ref. 43, Table IV.

[61] T. Tanaka and Y. Inuishi, J. Phys. Soc. Jap. **19**, 167 (1964).

[62] L. J. Cheng, J. C. Corelli, J. W. Corbett, and G. D. Watkins, Phys. Rev. **152**, 761 (1966).

[63] J. C. Corelli, R. C. Young, and C. S. Chen, IEEE Trans. Nucl. Sci. **17**, 128 (1970).

[64] C. A. J. Ammerlaan and G. D. Watkins, Phys. Rev. B **5**, 3988 (1972).

[65] D. K. Wilson, IEEE Trans. Nucl. Sci. **15**, 77 (1968).

PHYSICAL REVIEW B VOLUME 7, NUMBER 10 15 MAY 1973

Schottky-Barrier Electroreflectance: Application to GaAs

D. E. Aspnes and A. A. Studna

Bell Laboratories, Murray Hill, New Jersey 07974

(Received 9 November 1972)

We describe a Schottky-barrier electroreflectance (ER) technique for making high-resolution optical spectroscopic measurements on semiconducting materials. When combined with recent line-shape theories of low-field ER spectra, the method provides order-of-magnitude improvement in resolution of structure and accuracy in the determination of critical-point energies and broadening parameters as compared to previous spectroscopic work on higher interband transitions. The Schottky-barrier technique is applied to GaAs, where separate critical-point contributions of Γ and Δ symmetry in the E'_0 triplet are resolved for the first time, together with all members of the quadruplet at X. We find the values of critical-point energies E_g and broadening parameters Γ for the following transitions at 4.2 °K (all energies are in meV): $E_0(1517.7 \pm 0.5, < 0.3)$; $E_0 + \Delta_0(1859 \pm 1, 6 \pm 2)$; $E_1(3043.9 \pm 1, 28 \pm 1)$; $E_1 + \Delta_1(3263.6 \pm 1, 38 \pm 2)$; E'_0 triplet, Γ symmetry: $(4488 \pm 10, < 40 \pm 5)$, $(4659 \pm 10, 30 \pm 5)$, $(5014 \pm 15, 47 \pm 10)$; E'_0 triplet, M_1 transitions, Δ symmetry: $(4529 \pm 10, < 36 \pm 5)$ and $(4712 \pm 10, 34 \pm 5)$; E_2 complex, Σ: $(5137 \pm 10, 104 \pm 10)$; E_2 complex, X quadruplet: $(4937 \pm 10, 47 \pm 10)$, $(5014 \pm 10, 47 \pm 10)$, $(5339 \pm 10, 48 \pm 10)$, $(5415 \pm 15, 50 \pm 15)$. These values enable us to determine the following spin-orbit-splitting energies: $\Delta_0 = 341 \pm 2$ meV, $\Delta_1 = 220 \pm 2$ meV, $\Delta'_0(\text{at } \Gamma) = 171 \pm 15$ meV, $\Delta''_0(\text{at } \Delta) = 183 \pm 15$ meV, and $\Delta_2 = 77 \pm 10$ meV. The splitting of the lower conduction bands at X due to the antisymmetric potential is $\Delta'_2 = 402 \pm 10$ meV. The E'_0 transitions of Δ symmetry are shown to lie about 10% of the way from Γ to X. By comparing the period of the large number of Franz–Keldysh oscillations observed at the $E_1 + \Delta_1$ transition with those of the $E_0 + \Delta_0$ transitions observed in the high-field measurements, we determine a value $\mu_T = (0.055 \pm 008)m_e$ for the transverse reduced mass at $E_1 + \Delta_1$. These results are compared to previous experimental measurements and to calculated energy-band structures for GaAs. The determination of critical-point symmetry in surface-barrier geometries in terms of the transformation properties of the third- and fourth-rank low-field ER line-shape tensors is also discussed. Finally, the vanishing of an ER spectrum at a hyperbolic critical point, a reduced-mass effect predicted by the general theory of the Franz–Keldysh effect, is observed for the first time.

I. INTRODUCTION

Since the discovery of the electroreflectance (ER) effect in 1964,[1] numerous forms of modulation spectroscopy have been developed and great progress has been made in optical spectroscopy of solids.[2] As a result, much information has been obtained about the energy band structure and critical-point spectra of a wide variety of materials.[2,3] Recently, it has been shown that the sharp and richly structured ER spectra obtained at sufficiently low values of the modulating field arise from highly resonant fourth-rank-tensorial field-induced changes in the linear dielectric function.[4,5] These line shapes are closely related to the third derivative of the unperturbed dielectric function,[5-7] and thus are more directly suitable to high-resolution spectroscopy than other forms of modulation spectroscopy which yield broader first-derivative spectra.

Since low-field ER line shapes simply scale quadratically in the applied modulating field, depletion-barrier modulation is particularly well suited to high-resolution spectroscopy of semiconducting materials.[8] In addition to minimizing field-inhomogeneity effects,[9,10] the quadratic field dependence can be combined with the square-root dependence of the field on modulation potential in a fully depleted (nonequilibrium) space-charge region to yield spectra which are linear in the applied po-